2. Fundamentals of Boundary–Layer Theory

2.1 Boundary–Layer Concept

Flows of fluids with low viscosity values and thus very high Reynolds numbers occur in many technical applications. As was shown in the examples from the last chapter, the limiting solution $\mathrm{Re} = \infty$ is often a good approximation. A notable shortcoming of this limiting solution is that the no–slip condition is not satisfied, i.e. the velocities at the wall are not zero but are finite. The viscosity must be taken into account in order to satisfy the no–slip condition. This takes care of the velocity transition from the limiting solution's finite value close to the wall to the value of zero directly at the wall. At large Reynolds numbers this transition takes place in a thin layer close to the wall, called by L. Prandtl (1904) the *boundary layer* or *frictional layer*. As will be shown, the boundary layer is thinner the higher the Reynolds number, i.e. the smaller the viscosity.

The concept of the boundary layer, therefore, implies that flows at high Reynolds numbers can be divided up into two unequally large regions. In the bulk of the flow region, the viscosity can be neglected, and the flow corresponds to the inviscid limiting solution. This is called the inviscid outer flow. The second region is the very thin boundary layer at the wall where the viscosity must be taken into account.

Within the boundary layer the two different flow forms mentioned in the previous chapter can both occur, that is, the flow can be laminar or turbulent. One then speaks of laminar boundary–layer flows, or laminar boundary layers for short, and equivalently of turbulent boundary layers.

It will be seen later that the division of the flow field into the inviscid outer flow and the boundary layer leads to considerable simplifications in the theoretical treatment of high Reynolds number flows. In fact it is only due to this idea of Prandtl that any theoretical headway could be made on these flows at all.

Before coming to the focus of this book, the mathematical theory, this chapter will be used to explain the main concepts of boundary layers purely physically, without using any mathematical methods.

H. Schlichting (Deceased) and K. Gersten, Boundary-Layer Theory,
DOI 10.1007/978-3-662-52919-5_2

2.2 Laminar Boundary Layer on a Flat Plate at Zero Incidence

Figure 2.1 is a snapshot of the flow along a thin flat plate which is being dragged through water. Aluminium particles have been sprinkled on the surface of the water to make the streamlines visible. The length of each particle streak is proportional to the flow velocity. It can be seen that directly at the wall is a thin layer where the velocity is considerably lower than it is at some distance from the wall. The thickness of this layer increases along the plate from front to back. In Fig. 2.2 the velocity distribution in this boundary layer on the plate is shown schematically, where the dimension in the transverse direction is enlarged greatly. At the leading edge there is a constant velocity distribution perpendicular to the plate. As the distance from the leading edge gets larger, the layer of particles slowed down by the friction becomes ever larger, since more and more fluid particles are caught up by the retardation. The thickness of the boundary layer $\delta(x)$ is therefore a monotonically increasing function of x. Here, however, it must be made absolutely clear that the concept of boundary–layer thickness δ has been artificially introduced. The transition from boundary–layer flow to outer flow, at least in the case of laminar flows, takes place continuously, so that a precise boundary cannot, in principle, be given. Since the concept of boundary–layer thickness is so vivid, it is very often used in practice. Frequently the boundary is arbitrarily given as being at the point where the velocity reaches a certain percentage of the outer velocity, e.g. 99%. For clarity, an index is often used, e.g δ_{99}.

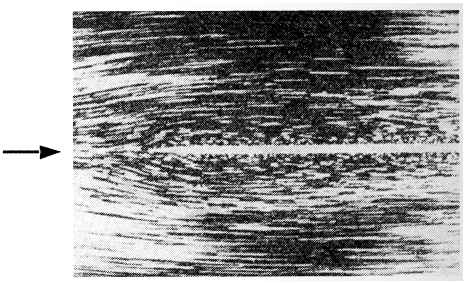

Fig. 2.1. Flow along a thin flat plate, after L. Prandtl; O. Tietjens (1931)

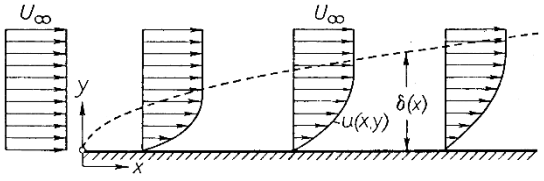

Fig. 2.2. Boundary layer at a flat plate at zero incidence (schematic)

Estimation of the boundary–layer thickness. For laminar plate boundary layers the boundary–layer thickness can easily be estimated as follows: in the boundary layer the inertial forces and the friction forces are in equilibrium. As was explained in Sect. 1.3, the inertial force per unit volume is equal to $\varrho u\,\partial u/\partial x$. For a plate of length x, $\partial u/\partial x$ is proportional to U_∞/x, where U_∞ is the velocity of the outer flow. Thus the inertial force is of the order of magnitude $\varrho U_\infty^2/x$. On the other hand, the friction force per unit volume is equal to $\partial\tau/\partial y$, and in laminar flows this is equal to $\mu\,\partial^2 u/\partial y^2$, by assumption. The velocity gradient perpendicular to the wall $\partial u/\partial y$ is of order U_∞/δ, so that for the friction force per unit volume $\partial\tau/\partial y \sim \mu U_\infty/\delta^2$. Setting the inertial and friction forces equal we reach the relation

$$\mu\frac{U_\infty}{\delta^2} \sim \frac{\varrho U_\infty^2}{x}$$

or, solved for the boundary–layer thickness δ:

$$\delta \sim \sqrt{\frac{\mu x}{\varrho U_\infty}} = \sqrt{\frac{\nu x}{U_\infty}}\ . \tag{2.1}$$

The unknown numerical factor remaining in this equation can be determined from the exact solution of H. Blasius (1908) which is fully treated in Chap. 6. For the laminar boundary layer at a plate at zero incidence we have:

$$\delta_{99}(x) = 5\sqrt{\frac{\nu x}{U_\infty}}\ . \tag{2.2}$$

The dimensionless boundary–layer thickness related to the plate length l is then

$$\frac{\delta_{99}(x)}{l} = \frac{5}{\sqrt{\mathrm{Re}}}\sqrt{\frac{x}{l}}\ , \tag{2.3}$$

where $\mathrm{Re} = U_\infty l/\nu$ is the Reynolds number formed with the plate length l. We see from Eq. (2.3) that the boundary–layer thickness decreases with increasing Reynolds number, so that in the limiting case $\mathrm{Re} = \infty$ the boundary layer does indeed vanish. In addition we see from Eq. (2.3) that the boundary–layer thickness grows in proportion to $\sqrt{x}$.

Displacement thickness. As already stated, the boundary–layer thickness has been introduced arbitrarily. A correct and fluid mechanically interpretable measure for the thickness of the boundary layer is the *displacement thickness* δ_1. It is defined by

$$U\delta_1(x) = \int_{y=0}^{\infty} (U-u)\,dy\ . \tag{2.4}$$

U is the velocity on the outer edge of the boundary layer at the position x. From this, the two shaded areas in Fig. 2.3 must be equal. The displacement

thickness tells us how far the streamlines of the outer flow are displaced by the boundary layer. For a plate at zero incidence we have

$$\frac{\delta_1(x)}{l} = \frac{1.721}{\sqrt{\mathrm{Re}}}\sqrt{\frac{x}{l}}\,, \tag{2.5}$$

i.e. the displacement thickness δ_1 is about 1/3 of the boundary–layer thickness δ_{99}.

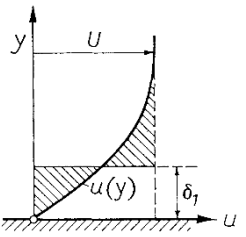

Fig. 2.3. Displacement thickness δ_1 of the boundary layer

Estimation of the friction forces. As with the boundary–layer thickness, the wall shear stress τ_w and thus the entire friction drag of the plate can also be estimated. According to Newton's law of friction, Eq. (1.2), we have:

$$\tau_\mathrm{w}(x) = \mu\left(\frac{\partial u}{\partial y}\right)_\mathrm{w}\,, \tag{2.6}$$

where the index w denotes the value at the wall. Using $\partial u/\partial y \sim U_\infty/\delta$ we find $\tau_\mathrm{w} \sim \mu U_\infty/\delta$, and inserting the value of δ from Eq. (2.1),

$$\tau_\mathrm{w}(x) \sim \mu U_\infty\sqrt{\frac{\varrho U_\infty}{\mu x}} = \sqrt{\frac{\mu\varrho U_\infty^3}{x}}\,. \tag{2.7}$$

Therefore the wall shear stress is proportional to $U_\infty^{3/2}$, and, particularly worth emphasising, to $1/\sqrt{x}$. The wall shear stress of a flat plate is therefore not a constant, but a function which decreases monotonically with x. The shear stresses are particularly large close to the leading edge of the plate. Using $\tau_\mathrm{w} \sim \mu U_\infty/\delta$ it follows that the wall shear stress is inversely proportional to the boundary–layer thickness, i.e. the thinner the boundary layer the higher the wall shear stress. The constant of proportionality in Eq. (2.7) can again be determined from the exact solution, see Chap. 6. Therefore the *skin–friction coefficient* is

$$c_f = \frac{\tau_\mathrm{w}(x)}{\frac{\varrho}{2}U_\infty^2} = \frac{0.664}{\sqrt{\mathrm{Re}}}\sqrt{\frac{l}{x}}\,. \tag{2.8}$$

Knowing the relation of the wall shear stress to position $\tau_w(x)$, integration can be used to determine the entire friction drag. A plate wetted on one side with breadth b and length l has a friction drag of

$$D = b \int_0^l \tau_w(x) dx \ . \tag{2.9}$$

With Eq. (2.8), the drag coefficient related to the wetted surface $S = b \cdot l$ follows as

$$c_D = \frac{D}{\frac{\varrho}{2} U_\infty^2 \cdot b \cdot l} = \frac{1.328}{\sqrt{\mathrm{Re}}} \ . \tag{2.10}$$

This drag law is depicted in Fig. 1.3. The asymptotic character of this law can be seen, and for Reynolds numbers $\mathrm{Re} > 10^4$ the measurements are very close to the theory.

2.3 Turbulent Boundary Layer on a Flat Plate at Zero Incidence

As was already mentioned in connection with Fig. 1.3, in reality the boundary layer on a plate does not always remain laminar. After a certain distance $x = x_{\mathrm{crit}}$ (from the leading edge of the plate), the boundary layer becomes turbulent. In analogy to Eq. (1.12), the *critical* Reynolds number formed with the distance to the transition point is

$$\mathrm{Re}_{\mathrm{x\,crit}} = \left(\frac{Ux}{\nu} \right)_{\mathrm{crit}} = 5 \cdot 10^5 \quad \text{(plate)} \ . \tag{2.11}$$

The boundary layer on a plate is laminar close to the leading edge and becomes turbulent further downstream, whereby the position of the transition point x_{crit} can be determined by the critical Reynolds number $\mathrm{Re}_{\mathrm{x\,crit}}$ given. Although the transition from laminar to turbulent is a region of finite length, a transition point is used for simplicity and it is frequently assumed that the transition is sudden (see the footnote on p. 437). The numerical value of $\mathrm{Re}_{\mathrm{crit}}$ is strongly dependent on how free from perturbation the outer flow is. In strongly perturbed flow $\mathrm{Re}_{\mathrm{crit}} = 3 \cdot 10^5$ is typical, whereas for particularly smooth flow values of $\mathrm{Re}_{\mathrm{crit}} = 3 \cdot 10^6$ have been reached, cf. Chap. 15.

The first investigations into the laminar–turbulent transition in the boundary layer were carried out by B.G. Van der Hegge Zijnen (1924), J.M. Burgers (1924) and M. Hansen (1928). The transition from laminar to turbulent flow forms is most noticeable by a great increase in the boundary–layer thickness and in the wall shear stress. Figure 2.4 shows the dimensionless combination $\delta_{99}/\sqrt{\nu x/U_\infty}$ depicted as a function of the dimensionless distance $\mathrm{Re}_x = U_\infty x/\nu$ according to measurements by M. Hansen (1928). From Eq. (2.2), in laminar boundary layers this combination has approximately the constant value 5. For $\mathrm{Re}_x = \mathrm{Re}_{\mathrm{x\,crit}} = 3 \cdot 10^5$, the measurements demonstrate

a strong sudden increase. As will be shown later in Sect. 18.2.5, the thickness of the turbulent boundary layer on the plate is:

$$\frac{\delta U_\infty}{\nu} = 0.14 \frac{\mathrm{Re_x}}{\ln \mathrm{Re_x}} \mathrm{G}(\ln \mathrm{Re_x}) \; . \tag{2.12}$$

The function $G(\ln \mathrm{Re_x})$ is only weakly dependent on $\ln \mathrm{Re_x}$. It has a limiting value of 1 for $\ln \mathrm{Re_x} \to \infty$; this will be discussed more fully in Sect. 17.1.3. In the region of interest here $10^5 < \mathrm{Re_x} < 10^6$, $G \approx 1.5$. The dependence on $\ln \mathrm{Re_x}$ which appears in Eq. (2.12) is typical for turbulent boundary layers, and has to do with an asymptotic formula for large Reynolds numbers. According to this formula, the boundary–layer thickness grows as $\delta \sim x/\ln x$ for large x. At a given x, the boundary–layer thickness decreases with increasing Reynolds number, but only very slowly with $\delta/x \sim 1/\ln \mathrm{Re}$. The combination corresponding to Eq. (2.12) shown in Fig. 2.4 shows good agreement with the measurements of M. Hansen. Since Eq. (2.12) holds for the case where a turbulent boundary layer is already present at the leading edge of the plate, a virtual origin of the boundary layer was assumed at $\mathrm{Re_x} = 1.5 \cdot 10^5$ in drawing the curve of Eq. (2.12). This means that precisely at the transition point $\mathrm{Re_x} = 3 \cdot 10^5$, the value of the combination is approximately 5.0, and therefore a continuous transition of the boundary layer from laminar to turbulent follows. The boundary–layer thicknesses for typical cases of water and air flows have been calculated from Eq. (2.12) and are given in Table 2.1.

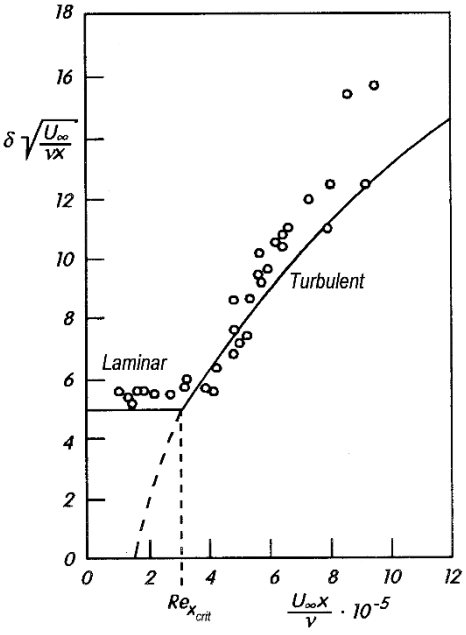

Fig. 2.4. Dependence of the boundary–layer thickness on the distance along a plate at zero incidence, after M. Hansen (1928)
laminar: Eq. (2.2)
turbulent: Eq. (2.12) with fictitious origin at $\mathrm{Re_x} = 1.5 \cdot 10^5$

Friction forces. As will also be shown in Sect. 18.2.5, the formula analogous to Eq. (2.8) for the skin–friction coefficient of a turbulent boundary layer reads

$$c_f = 2\left[\frac{\kappa}{\ln \mathrm{Re_x}}\mathrm{G}(\ln \mathrm{Re_x})\right]^2 , \tag{2.13}$$

where $\mathrm{G}(\ln \mathrm{Re_x})$ is again the function mentioned in connection with Eq. (2.12). The quantity $\kappa = 0.41$, called the Karman constant, is of fundamental importance for all turbulent wall boundary layers. It is a universal constant. From Eq. (2.13), the skin–friction coefficient for turbulent plate boundary layers decreases with increasing Reynolds number, but it does this extremely slowly, even more slowly than any small negative power of the Reynolds number. Assuming a turbulent boundary layer from the leading edge of the plate on, integration of the skin–friction coefficient over the length of the plate l gives the drag coefficient for a plate wetted on one side:

$$c_D = 2\left[\frac{\kappa}{\ln \mathrm{Re}}\mathrm{G}(\ln \mathrm{Re})\right]^2 , \tag{2.14}$$

where the Reynolds number Re is now formed with the plate length l. This function is shown in Fig. 1.3. The drag coefficient also decreases extremely slowly with increasing Reynolds number. Note that the functions G in Eqs. (2.13) and (2.14) are different, cf. Sect. 18.2.5.

Viscous sublayer. A peculiarity of turbulent boundary layers will be indicated at this point. In laminar boundary layers, the boundary layer is the region in the flow field affected by the viscosity, but this is not the case in turbulent boundary layers. The entire flow field is now divided into the outer flow, free from turbulence (or at least lacking in turbulence), and the turbulent flow, characterised by random fluctuating motion, inside the boundary layer. Since "apparent" friction forces occur in the turbulent boundary layer, as will be shown in Chap. 18, a turbulent boundary layer is also called a frictional layer. Within this turbulent frictional layer, the effect of the viscosity is restricted to a layer directly at the wall which is much thinner than the boundary layer. This is called the *viscous sublayer* or *viscous wall layer*. Therefore the turbulent boundary layer has a double layered structure. The larger part is a frictional layer only because of the "apparent friction" due to the turbulent fluctuating motion, and is unaffected by the viscosity. In the very thin viscous sublayer, the effects of the viscosity are in the form of "true" friction forces.

Although the transition between the two layers is continuous here too, in practice the concept of the thickness of the viscous sublayer δ_v is used. As will be shown in Sect. 17.1.2

$$\frac{\delta_v}{x} = \frac{50}{\mathrm{Re_x}\sqrt{\frac{c_f}{2}}} , \tag{2.15}$$

where the skin–friction coefficient c_f is given by Eq. (2.13). From this, $\delta_v \sim \ln x$ grows very slowly with distance from the leading edge. It also decreases with increasing Reynolds number at a fixed x as $\delta_v \sim \ln \mathrm{Re_x}/\mathrm{Re_x}$.

The ratio of the sublayer thickness δ_v to the total thickness δ follows from Eqs. (2.12) and (2.15)

$$\frac{\delta_v}{\delta} = 680 \frac{\ln^2 \mathrm{Re_x}}{\mathrm{Re_x}} \,. \tag{2.16}$$

As $\mathrm{Re_x}$ increases, the part of the total frictional layer that makes up the viscous sublayer gets ever smaller.

Numerical examples of the absolute thickness of the sublayer are given in Table 2.1.

Table 2.1. Boundary–layer thickness δ and thickness of the viscous sublayer δ_v at the end of a flat plate at zero incidence in turbulent flow according to Eqs. (2.12) and (2.15). l: plate length, U_∞: free stream velocity, ν: kinematic viscosity

	$\frac{U_\infty}{\mathrm{m/s}}$	$\frac{l}{\mathrm{m}}$	$\mathrm{Re} = \frac{U_\infty l}{\nu}$	$\frac{\delta}{\mathrm{mm}}$	$\frac{\delta_v}{\mathrm{mm}}$
	50	1	$3.3 \cdot 10^6$	8	0.4
air	100	1	$6.6 \cdot 10^6$	8	0.2
$\nu = 15 \cdot 10^{-6} \frac{\mathrm{m}^2}{\mathrm{s}}$	100	5	$3.3 \cdot 10^7$	36	0.2
	200	10	$1.3 \cdot 10^8$	69	0.1
	1	2	$2 \cdot 10^6$	17	1
water	2	5	$1 \cdot 10^7$	39	0.6
$\nu = 10^{-6} \frac{\mathrm{m}^2}{\mathrm{s}}$	5	50	$2.5 \cdot 10^8$	321	0.4
	10	200	$2 \cdot 10^9$	1122	0.1

2.4 Fully Developed Turbulent Flow in a Pipe

In Chap. 1, in connection with Fig. 1.4., mention has already been made of fully developed turbulent flow in a pipe. This case of an internal flow is initially not a flow with typical boundary–layer character. However it has, just like the turbulent frictional layer described in the previous section, a double layer structure with a turbulent core and a viscous sublayer. As the Reynolds number increases, the thickness of the sublayer decreases, so that the final limiting solution is of a flow with homogeneous velocity. In this manner this flow can also be treated using the methods of boundary–layer theory.

Pipe friction factor. The pipe friction factor λ depicted in Fig. 1.4 is defined as follows:

$$\lambda = -\frac{d}{\frac{\varrho}{2}u_m^2}\frac{dp}{dx} = \frac{4\bar{\tau}_\mathrm{w}}{\frac{\varrho}{2}u_m^2} \,. \tag{2.17}$$

As will be shown in Sect. 17.2.3, in the case of a smooth surface, the dependence on the Reynolds number $\mathrm{Re} = u_m d/\nu$ is given by:

$$\lambda = 8\left[\frac{\kappa}{\ln \mathrm{Re}}\mathrm{G}(\ln \mathrm{Re})\right]^2 \,. \tag{2.18}$$

Here $\mathrm{G}(\ln \mathrm{Re})$ is again a function which monotonically decreases with increasing $\ln \mathrm{Re}$, and which has a limit of 1 for $\mathrm{Re} \to \infty$. In the region of interest in practice, $2300 < \mathrm{Re} < 10^7$, its value is about $\mathrm{G} = 1.35$. The law of friction in Eq. (2.18) is shown in Fig. 1.4, and agrees well with experimental results.

Thickness of the viscous sublayer. The thickness of the viscous sublayer can also be determined approximately (see Chap. 17):

$$\frac{\delta_v}{d} = 122\frac{\ln \mathrm{Re}}{\mathrm{Re}\,\mathrm{G}(\ln \mathrm{Re})} \,. \tag{2.19}$$

As already mentioned, the thickness of the viscous sublayer decreases to zero with increasing Reynolds number. Numerical values of δ_v are given for practical examples of turbulent pipe flows of air and water in Table 2.2.

Table 2.2. Thickness of the viscous sublayer δ_v in fully developed turbulent pipe flow (smooth surface), according to Eq. (2.19)

	$\frac{u_m}{\mathrm{m/s}}$	$\frac{d}{\mathrm{m}}$	Re	G	$\frac{\delta_v}{\mathrm{mm}}$
	3	0.01	$2 \cdot 10^3$	1.47	3.2
	3	0.1	$2 \cdot 10^4$	1.38	4.4
air	3	1.0	$2 \cdot 10^5$	1.33	5.6
$\nu = 15 \cdot 10^{-6}\frac{\mathrm{m}^2}{\mathrm{s}}$	30	0.01	$2 \cdot 10^4$	1.38	0.4
	30	0.1	$2 \cdot 10^5$	1.33	0.6
	30	1.0	$2 \cdot 10^6$	1.39	0.7
	0.2	0.01	$2 \cdot 10^3$	1.47	3.2
	0.2	0.1	$2 \cdot 10^4$	1.38	4.4
water	0.2	1.0	$2 \cdot 10^5$	1.33	5.6
$\nu = 10^{-6}\frac{\mathrm{m}^2}{\mathrm{s}}$	20	0.01	$2 \cdot 10^5$	1.33	0.06
	20	0.1	$2 \cdot 10^6$	1.29	0.07
	20	1.0	$2 \cdot 10^7$	1.26	0.08

2.5 Boundary Layer on an Airfoil

The boundary layers on flat plates at zero incidence treated in Sects. 2.2 and 2.3 were particularly simple, since the inviscid outer flow and thus the limiting solution were translation flows with constant pressure in the entire field. However, in the case of flow past an arbitrarily shaped body, additional pressure forces occur. Figure 2.5 shows the boundary layer on an airfoil, where, for reasons of clarity, the dimension in the transverse direction is enlarged greatly. As with the plate, a laminar boundary layer begins to develop at the nose of the airfoil. After a certain distance x_{crit} along the contour of the body, the laminar–turbulent transition occurs, so that the boundary layer is turbulent for $x > x_{\mathrm{crit}}$. Because of the geometry of the body, the invis-

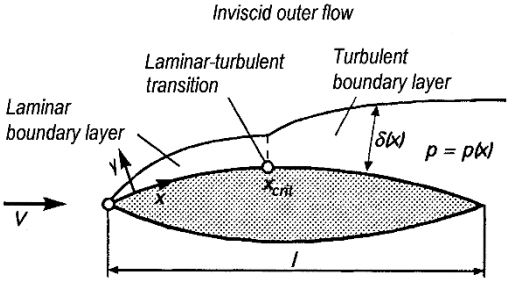

Fig. 2.5. Development of the boundary layer at an airfoil

cid outer flow gives rise to a pressure distribution on the outer edge of the boundary layer. This pressure distribution is "imposed" onto the boundary layer, i.e. at every point x, the pressure in the boundary layer perpendicular to the wall is constant. Therefore the pressure distribution on the outer edge of the boundary layer is identical to the pressure distribution at the wall. Any differences between these two pressure distributions could only arise from streamline curvature and the resulting pressure gradients perpendicular to the main flow direction as a compensation for centrifugal forces. Since boundary layers are very thin compared to the radius of curvature of the body's contour at high Reynolds numbers, to first order, pressure gradients perpendicular to the wall do not occur. The pressure is imposed on the boundary layer by the outer flow and is only a function of x. Additionally, the dependencies mentioned in the case of the plate boundary layer are also valid: as the boundary layer develops along the contour of the body, in general the boundary–layer thickness $\delta(x)$ increases and the wall shear stress τ_{w} decreases. The increase in boundary–layer thickness downstream is greater in the case of turbulent boundary layers than laminar. As the Reynolds number formed with the free stream velocity V and a characteristic length of the body l increases, the thickness of the boundary layer decreases to zero in the limiting case $\mathrm{Re} \to \infty$. The pressure distribution imposed by the outer flow is of considerable importance in the formation of the boundary layer. For

example, the position of the laminar–turbulent transition depends strongly on it. If the pressure greatly increases in the flow direction, as can occur in the region towards the back of the airfoil, or on the back of blunt bodies, it is possible that the boundary layer can separate from the wall. This extremely important phenomenon of boundary–layer separation will be treated in more detail in the next section.

2.6 Separation of the Boundary Layer

In order to explain the important phenomenon of boundary–layer separation, let us consider the flow past a blunt body, e.g. past a circular cylinder as in Fig. 2.6. In inviscid symmetric flow (Fig. 1.14a), an accelerated flow with pressure drop is present on the front half from D to E; from E to F on the back there is a decelerated flow with pressure increase. After setting the flow in motion, as long as the boundary layer remains very thin, an almost inviscid flow first forms. For a particle in the outer flow moving from D to E, pressure is transformed into kinetic energy, and moving from E to F, kinetic energy is transformed into pressure. A fluid particle directly at the wall in the

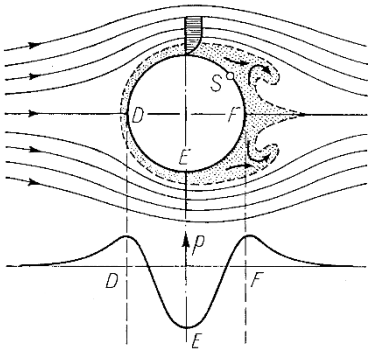

Fig. 2.6. Separation of the boundary layer and vortex formation at a circular cylinder (schematic). S = separation point

boundary layer is also acted on by the same pressure distribution as in the outer flow, since this is imposed on the boundary layer. Because of the strong friction forces in the thin frictional layer, a boundary–layer particle loses so much of its kinetic energy that it cannot manage to get over the "pressure mountain" from E to F. Such a particle cannot make much headway into the region of increasing pressure from E to F. It comes to a standstill, and is pushed backwards into motion by the pressure distribution of the outer flow. The flow portraits in Fig. 2.7 are a time sequence of this process on the back of a blunt body. The pressure increases along the contour of the body from left to right. The flow has been made visible by little particles of aluminium which have been sprinkled onto the surface of the water. The

boundary layer is easily seen in the figures by the short streaklines of the particles. In Fig. 2.7a (shortly after starting) the reversed motion has just begun at the trailing edge. In Fig. 2.7b, the boundary layer has thickened, and the start of the reversed motion has moved forward considerably. It can be seen from Fig. 2.7c that a large vortex has formed from the backflow, and this is even larger in Fig. 2.7d. This vortex then soon separates from the body and moves on downstream. This process changes the flow portrait at the back of the body fully and the pressure distribution is drastically changed compared to that of inviscid flow. The final flow state for the cylinder can be seen in Fig. 1.16. As the pressure distribution in Fig. 1.13 shows, there is quite a strong negative pressure in the region filled with vortices. This negative pressure is the origin of the large form drag of the body.

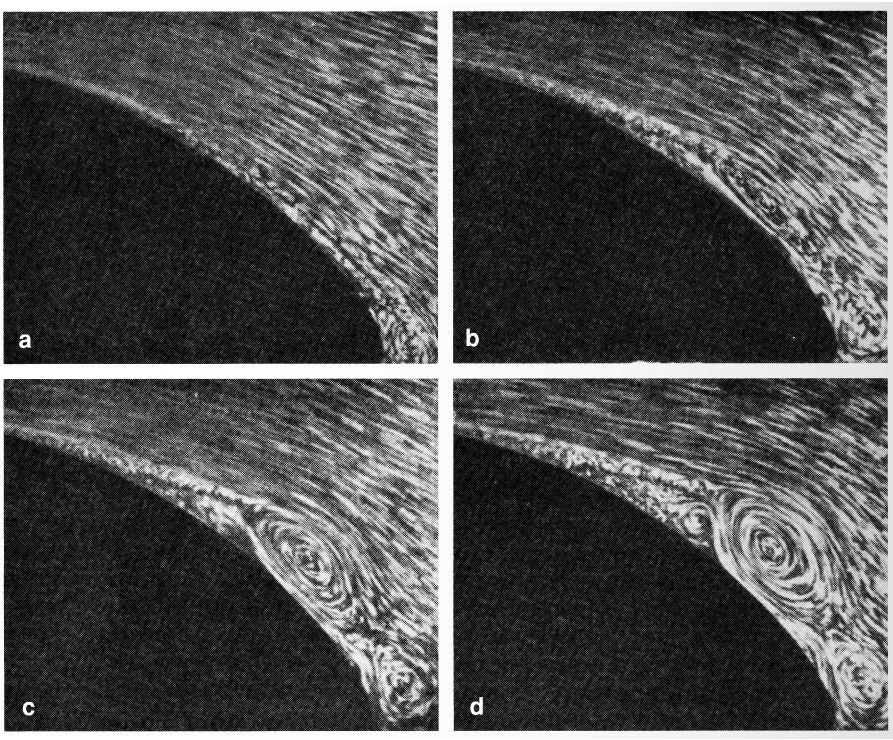

Fig. 2.7 a-d. Development in time of the separation at the back of a blunt body, after L. Prandtl; O. Tietjens (1931)

Separation condition. As well as the friction drag, boundary–layer theory is also able, via the separation process, to explain the form drag (pressure drag). There is always danger of separation in regions where the pressure increases, and it is even greater the larger the increase, particularly for bodies with blunt rear sides. We can now understand why the pressure distribution

observed in Fig. 1.8 for the slender airfoil agrees so well with the theoretical inviscid flow. The pressure increase at the back is so weak that the boundary layer does not separate. As a result, not much form drag occurs and the total drag consists mainly of the friction drag and remains therefore small.

The flow portrait of boundary–layer flow close to separation is of the kind depicted in Fig. 2.8. As a result of the backflow close to the wall, a strong thickening of the boundary layer takes place and with this, boundary–layer mass is transported away into the outer flow. At the point of separation, the streamlines leave the wall at a certain angle. The position of separation is given by the condition that the velocity gradient perpendicular to the wall vanishes at the wall, i.e. the wall shear stress τ_w vanishes:

$$\tau_w = \mu \left(\frac{\partial u}{\partial y} \right)_w = 0 \quad \text{(separation)} \, . \tag{2.20}$$

The position of separation can only be determined by exact calculation (integration of the boundary–layer differential equations).

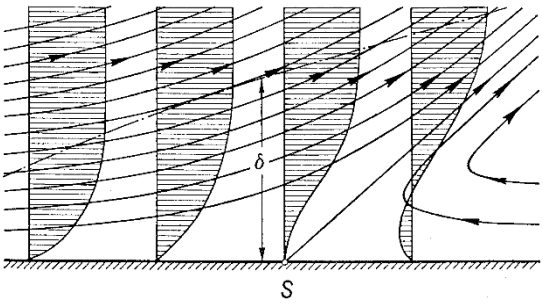

Fig. 2.8. Boundary–layer flow close to the separation point (schematic). S = separation point

The same process of separation discussed for flow past a circular cylinder also occurs in a channel which widens in the direction of flow (diffuser) (Fig. 2.9a). Up until the narrowest cross–section the pressure drops in the direction of flow. Here the flow is right along the walls, just as in inviscid flow. After the narrowest point, the expansion is so great and therefore the pressure increase so large that the boundary layer separates from both walls. The flow now only fills a small part of the cross–section of the channel. However, if the boundary layer is sucked away at the walls (Figs. 2.9b and 2.9c), the separation comes to a stop.

The flow portraits in Fig. 2.10 show that the pressure gradient along the wall acts together with the friction along the wall to govern the separation process. The picture on the left shows the flow against a wall placed perpendicular to it (plane stagnation–point flow). On the streamline of symmetry which leads to the stagnation point, there is a strong pressure increase in the direction of flow. However, there is no separation here because there is

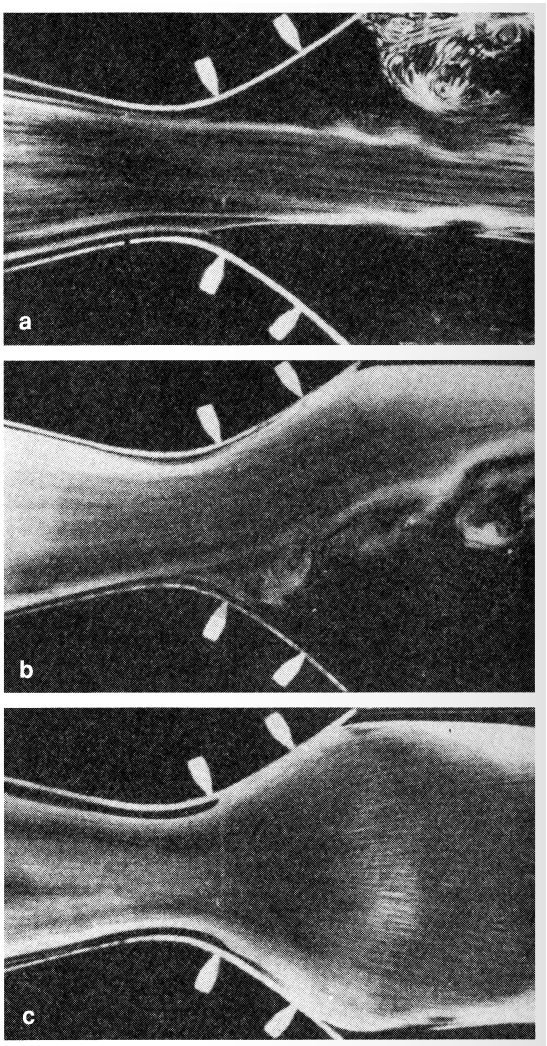

Fig. 2.9. Flow in a widening channel (diffuser) (**a**) separation at both diffuser walls, (**b**) suction of the boundary layer at the upper diffuser wall, (**c**) suction at both diffuser walls (after L. Prandtl; O. Tietjens (1931))

no wall friction present. There is even no separation at the wall itself, because here the boundary layer in both directions flows in the direction of falling pressure. If a very thin wall is now placed at right angles to the first wall at the stagnation point (Fig. 2.10b), it now has on it a boundary layer with increasing pressure in the flow direction. Because of this, the boundary layer here separates from the flat wall.

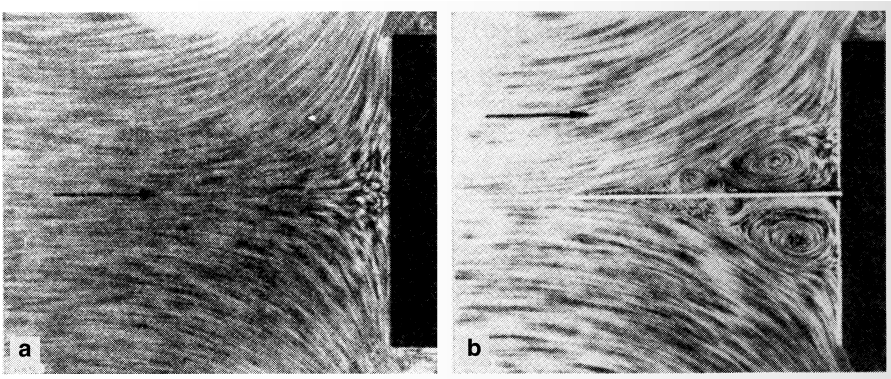

Fig. 2.10. Stagnation point flow, after H. Föttinger (1939), (**a**) free stagnation–point flow without separation, (**b**) retarded stagnation–point flow, with separation

The flow separation is frequently quite sensitive to small changes in the shape of the body, particularly if the pressure distribution is strongly affected by the change of shape of the body.

Other examples of separation. An instructive example is to be found in the flow portraits of the model of a motor vehicle (a VW–van) shown in Fig. 2.11 (E. Möller (1951), H. Schlichting (1954)). If the front of the van is square (a), the flow past the sharp front edge produces strong negative pressures and therefore a strong increase in pressure along the side walls. This leads to a complete separation of the boundary layer along the whole side wall and therefore to a large "dead water" area behind the body. The drag coefficient for this van with a square front is $c_D = 0.76$. For a rounded front (b), on the other hand, the strong negative pressures at the front edge are avoided and a flow attached to the entire side wall is achieved. There is a considerable reduction in the drag coefficient to $c_D = 0.42$. Further detailed investigations on such vehicles, also for asymmetric free streams, have been carried out by W.H. Hucho (1972, 1981).

Separation is also important in the production of lift on an airfoil. At small angles of attack (up to about 10°), the flow moves along both sides without separation, so that, to good approximation, an inviscid lift–producing flow is found. This pressure distribution was given in Fig. 1.9 (attached flow, Fig. 2.12a). As the angle of attack is increased, there is danger of separation

on the suction side. This is because the pressure increase is greater here. At a certain angle of attack, about 15°, separation occurs. The position of separation is quite close to the nose of the airfoil. The separated flow (Fig. 2.12b) has a large area of "dead water". The inviscid lift–producing flow has been destroyed and the drag is now very high. The start of separation coincides approximately with the maximum lift of the airfoil.

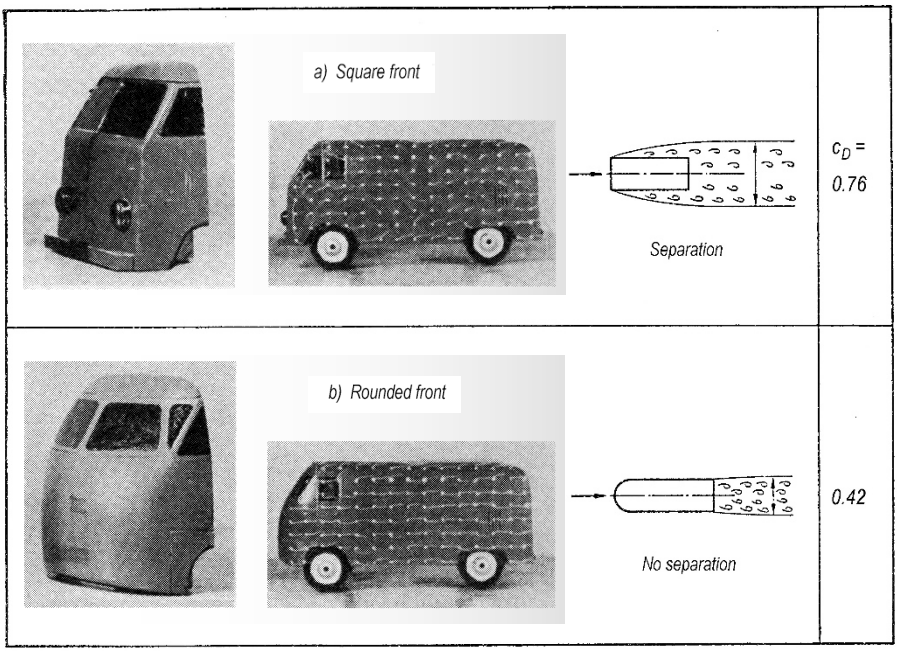

Fig. 2.11. Flow past a model of a vehicle (Volkswagen van), after E. Möller (1951). (**a**) Square front with fully separated flow along the entire side walls and large drag coefficient $c_D = 0.76$. (**b**) Rounded front with attached flow along the entire side wall and small drag coefficient $c_D = 0.42$.

Boundary–layer separation can even play a role when the angle of attack on an airfoil is moderate, if flow close to the speed of sound is considered. As already explained in Fig. 1.11, a shock generally forms on the suction side of the airfoil. If the shock is strong enough, the pressure distribution it causes can lead the boundary layer to separate. Because of the additional form drag occurring, a drastic increase of the drag can take place close to the speed of sound; this is frequently called the "sound barrier".

Finally we present a particularly instructive example of how the drag of a body can be dramatically decreased if the separation of the boundary layer is completely avoided and additionally if the shape is suitably chosen. Figure 2.13 shows the effect of a suitable shaping (streamline form) on the drag: the

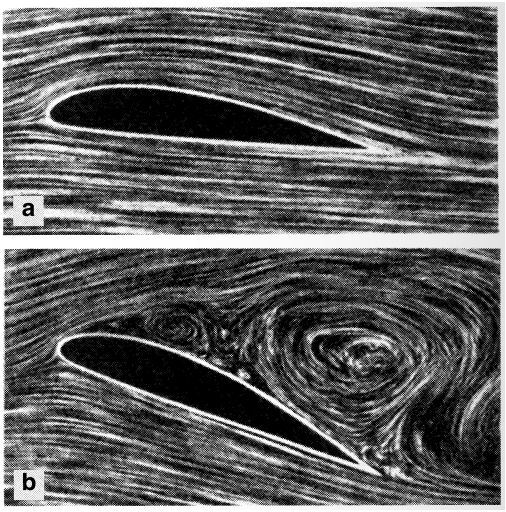

Fig. 2.12. Flow past an airfoil, (**a**) attached flow, (**b**) separated flow, after L. Prandtl; O. Tietjens (1931)

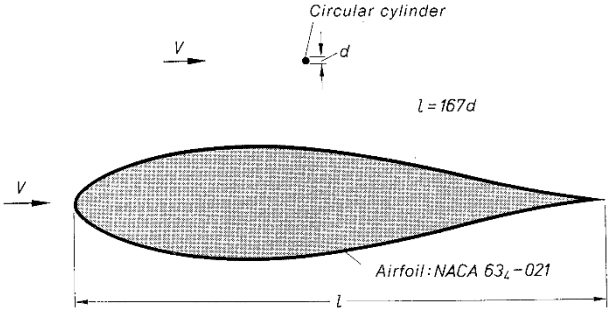

Fig. 2.13. Relative sizes of an airfoil and a circular cylinder at equal free stream velocities (parallel to the symmetry axis of the airfoil) which have the same drag.
Airfoil: laminar airfoil NACA $63_4 - 021$ with laminar boundary layer. Drag coefficient $c_D = 0.006$ at $\mathrm{Re}_l = 10^6$ to 10^7
Circular cylinder: drag coefficient $c_D = 1.0$ at $\mathrm{Re}_l = 10^4$ to 10^5 (Fig. 1.12)
The ratio of the chord of the airfoil l to the diameter of the cylinder d has the value $l/d = 1.0/0.006 = 167$

relative sizes of a symmetric airfoil and a circular cylinder (a thin wire) are sketched such that they have the same drag at the same free stream velocity. The cylinder has a drag coefficient of about $c_D \approx 1$, related to its frontal area, cf. Fig. 1.12. The airfoil has a very small drag coefficient of $c_D \approx 0.006$, related to its outline area. This extremely small drag coefficient was achieved by the fact that, because of suitable shaping, the boundary layer remains laminar almost along the entire length (laminar airfoil); see alse Chap. 15, in particular Fig. 15.27.

Difference between laminar and turbulent boundary–layer separation. A particularly remarkable phenomenon connected with the laminar–turbulent transition in boundary layers occurs at blunt bodies, such as cylinders and spheres. It can be seen from Figs. 1.12 and 1.19 that, for Reynolds numbers Vd/ν of about $5 \cdot 10^5$ and $3 \cdot 10^5$ respectively, a sudden large drop in the drag coefficient takes place. This was first noted for spheres by G. Eiffel (1912), and has to do with the fact that the boundary layer becomes turbulent. The point of separation thus is moved further backwards, since, because of the turbulent mixing motion, the energizing action of the outer flow on the turbulent boundary layer is much greater than in the laminar case. The separation point for laminar flow lies approximately at the equator, but when the boundary layer becomes turbulent, the point is moved some distance downstream. Thus the "dead water" area behind the body becomes considerably narrower, and the pressure distribution becomes closer to that of inviscid flow (Fig. 1.17). As the dead water area shrinks, a considerable lessening of the form drag takes place, seen as a jump in the curve $c_D = f(\mathrm{Re})$. L. Prandtl (1914) was able to show that this is the correct explanation by placing a thin wire ring around the sphere just in front of the equator (a "trip wire"). This artificially makes the laminar flow turbulent at a lower Reynolds number, and the same drop in drag which normally only happens at higher Reynolds numbers occurs. Figure 2.14 shows flow portraits where the flows have been made visible with smoke. On the left is a sphere in subcritical flow state, with a large dead water area and drag, and on the right, the supercritical state with small dead water area and drag. The second state has been produced using Prandtl's trip wire. This experiment shows clearly that the jump in the resistance curve of the sphere and cylinder can only be understood as a boundary–layer effect.

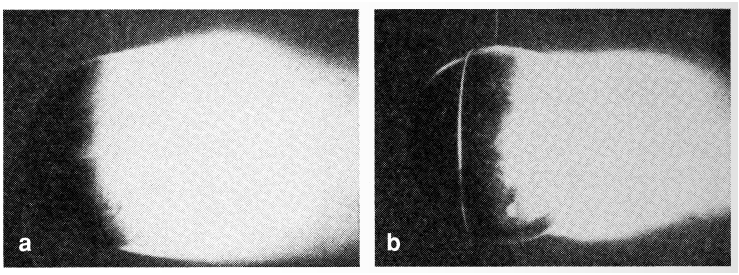

Fig. 2.14. Flow past a sphere, according to C. Wieselsberger (1914). (**a**) subcritical flow in subcritical Reynolds number regime, (**b**) supercritical flow in subcritical Reynolds number regime. Applying a thin trip wire enforces the subcritical flow

Other bodies which have a blunt rounded back side (e.g. elliptic cylinders) show in principle a similar drag coefficient dependence on the Reynolds number. For ever narrower bodies, the jump in the drag curve moves back further and further. In the case of a slender airfoil (Fig. 1.8), where basically

no boundary–layer separation takes place, there is also no jump in the c_D curve. The smooth increase in pressure on the back of this body is overcome by the boundary layer without separation. As we will see more clearly later, the pressure in the outer flow has an important effect on the position of the laminar–turbulent transition. In the area from the nose to the pressure minimum where the pressure decreases, the boundary layer is laminar, whereas from then on, in the region of rising pressure, it is mostly turbulent. It is important to note that separation can in general only be prevented if the flow in the boundary layer is turbulent. As will be seen later, a laminar boundary layer can tolerate only an extremely small pressure rise, so that separation occurs even if the body is very slender. This is particularly true even for airfoil flow with a pressure distribution as in Fig. 1.9. The danger of separation is largest here on the suction side. Here too, smooth, separation–free, lift–producing flow is only possible if the boundary–layer flow is turbulent. This can be summarised by saying that both the small drag of slender bodies as well as the lift of airfoils are generally due to the turbulence in the boundary layer.

One particular difference between laminar and turbulent boundary–layer separation should also be mentioned here. After the boundary layer has separated and left the body, it develops into so–called *free shear layers* further downstream, and forms the wake. In the limiting case $\mathrm{Re} = \infty$, the laminar free shear layers reduce to lines and surfaces of discontinuity, cf. Fig. 1.14b. In contrast, the turbulent free shear layers have a finite thickness at $\mathrm{Re} = \infty$. If turbulent free shear layers form from separation, the limiting solution at $\mathrm{Re} = \infty$ has no viscosity, but does have friction: an apparent friction, due to the turbulent fluctuating motion, exists.

Unsteady wakes. As already discussed in Chap. 1 in connection with the flow past a cylinder (Figs. 1.15 and 1.16 and Table 1.1), in spite of steady free stream conditions, the flow after separation is in no way steady. By this we mean varying processes in the mean motion, which move slowly compared to any turbulent fluctuating processes. This phenomenon does not only occur in the case of a circular cylinder, but also in the cases of blunt bodies of arbitrary shape and airfoils at large angles of attack. Sometimes a regular arrangement of vortices rotating clockwise and anticlockwise appears behind the body; this is known as the *Karman vortex street*. The unsteady character of the wake clearly has a great effect on the drag of the body, cf. Fig. 1.15. Understandably, in particular cases it is extremely difficult to establish whether unsteady flow takes place, and how it is to be determined. Research into this is still very much underway: see the summaries by L. Rosenhead (1931/32), M.V. Morkovin (1964), R. Wille (1966), E. Berger; R. Wille (1972), T. Sarpkaya (1975), W.J. McCroskey (1977), H.W. Förstching (1978) and D.P. Telionis (1981), as well as H. Schlichting (1982).

Measures to prevent separation. The separation of the boundary layer is generally undesirable, since it leads to great losses in energy. Certain measures have been devised to artificially prevent separation of the boundary layer.

It is physically easiest to *move the wall* in the flow direction too and thus to remove the velocity difference between wall and outer flow, the origin of boundary–layer formation. Of course, technically this is very difficult to realise. However L. Prandtl; O. Tietjens (1931) used a *rotating cylinder* to show that this method does work: on the side where the motion of the wall and the outer flow are the same there is no boundary–layer separation at all.

Another useful method to prevent boundary–layer separation is *suction*. The slowed boundary–layer material is sucked into the inside of the body through narrow slits on the wall. If the suction is strong enough, boundary–layer separation can be prevented. Boundary–layer suction was applied by L. Prandtl in 1904 in his first fundamental work on boundary layers on a circular cylinder. Separation can almost be completely prevented by suction through a slit on the back of the cylinder. Figure 2.9 shows an example of boundary–layer suction on the flow in a greatly diverging channel. Without suction there is strong separation (Fig. 2.9a). When suction is applied only on one side, the flow moves along this wall (Fig. 2.9b) and when suction is set in motion on both sides, the flow fills up the entire channel (Fig. 2.9c). We then obtain the flow portrait for inviscid flow. Suction has been used effectively to increase the lift on airfoils too. Applied to the back of the upper side, suction can be used to keep the flow along side the airfoil at much larger angles of attack than otherwise. This leads to a considerable increase in the maximum lift, O. Schrenk (1935).

Separation of the boundary layer can also be prevented by *blowing* tangentially into the boundary layer. Using a "wall jet" blown through a slit on the contour of the boundary layer parallel to the main flow direction, the boundary layer can be given enough kinetic energy to prevent separation. The maximum lift can be considerably increased using this principle.

In principle, a *slat* can be used on airfoils to prevent separation. In this case the pressure distribution on the airfoil is suitably influenced by the presence of the slat. Positive pressure gradients are avoided and thus separation prevented.

A summary of flow separation and its control may be found in P.K. Chang (1970), P.K. Chang (1976).

2.7 Overview of the Following Material

Now that we have briefly presented the essential physical fundamentals of flows with very low viscosity, the rational theory of these phenomena will be developed from the fluid–dynamic equations of motion of viscous fluid flows. This will be organised as follows: in Part I the general Navier–Stokes equations are derived. From these, in Part II Prandtl's boundary–layer equations

will be derived, based on the simplifications which follow from the smallness of the viscosity. The theory of integrating the boundary–layer equations for laminar flows will follow this. The problem of the onset of turbulence (laminar–turbulent transition) will be treated in Part III. Part IV will consist of the boundary–layer theory of fully developed turbulent flows. While the theory of laminar boundary layers can be treated purely by deduction from the Navier–Stokes differential equations, this has not been possible in the case of turbulent flows. Because they are so complicated, a purely theoretical approach is not possible. The theoretical treatment of turbulent flows therefore must depend on experimental results, and it is therefore a semi–empirical theory. The numerical methods of boundary–layer theory are treated in Part V.

http://www.springer.com/978-3-662-52917-1

Boundary-Layer Theory
Schlichting (Deceased), H.; Gersten, K.
2017, XXVIII, 805 p. 288 illus., Hardcover
ISBN: 978-3-662-52917-1